STRUCTURAL BIOLOGY COMMUNICATIONS

ISSN 2053-230X

X-ray structure of a human cardiac muscle troponin C/troponin I chimera in two crystal forms

Chunhong Yan and John S. Sack*

Small Molecule Drug Discovery, Bristol Myers Squibb Research and Development, PO Box 4000, Princeton, NJ 08543-4000, USA. *Correspondence e-mail: sackjs@gmail.com

Received 27 September 2021
Accepted 22 November 2021

Edited by R. L. Stanfield, The Scripps Research Institute, USA

Keywords: human cardiac muscle troponin C; troponin C/troponin I chimera; calcium regulation; cardiac muscle contraction.

PDB references: N-domain of cardiac muscle troponin C tethered to the switch region of cardiac muscle troponin I, tetragonal form, 7sc2; orthorhombic form, 7sc3

Supporting information: this article has supporting information at journals.iucr.org/f

The X-ray crystal structure of a human cardiac muscle troponin C/troponin I chimera has been determined in two different crystal forms and shows a conformation of the complex that differs from that previously observed by NMR. The chimera consists of the N-terminal domain of troponin C (cTnC; residues 1–80) fused to the switch region of troponin I (cTnI; residues 138–162). In both crystal forms, the cTnI residues form a six-turn α-helix that lays across the hydrophobic groove of an adjacent cTnC molecule in the crystal structure. In contrast to previous models, the cTnI helix runs in a parallel direction relative to the cTnC groove and completely blocks the calcium desensitizer binding site of the cTnC–cTnI interface.

1. Introduction

The role of the troponin complex in the calcium regulation of cardiac muscle contraction has been well established (for a review, see Marston & Zamora, 2020). The binding of calcium to troponin C (cTnC) allows a conformational change in the protein to occur, exposing a hydrophobic pocket and permitting troponin I (cTnI) to bind, releasing it from actin and leading to muscle contraction. An understanding of the molecular interactions involved in the calcium regulation of troponin, and in particular the interactions between the cTnC and cTnI subunits, may aid in the design of drugs that modulate this activation in the treatment of heart failure and other cardiomyopathies.

Multiple techniques have been used to understand the structural basis of the cTnC–cTnI interaction. The solution structure of the N-terminal domain of human cardiac cTnC with the cTnI C-terminal 'switch' peptide (residues 147–163), determined by NMR spectroscopy (Li *et al.*, 1999), shows that cTnC is in the open, Ca^{2+}-saturated, conformation. The cTnI peptide forms a partial eight-residue α-helical conformation, binding across the face of cTnC and making numerous hydrophobic interactions with the N-terminal region of cTnC. The cTnI α-helical peptide runs in a 'head-to-tail' or 'anti-parallel' orientation relative to the cTnC domain and the C-terminal portion of cTnI peptide is disordered.

The X-ray crystal structure of the core domain of the human cardiac troponin complex, containing both domains of the cTnC subunit and the larger portion of the cTnI subunit, as well as a portion of the troponin T subunit, has been determined to 2.6 Å resolution (Takeda *et al.*, 2003). The structure shows a cTnC–cTnI interaction similar to that seen in the NMR structure, including a ten-residue cTnI α-helix running antiparallel to the hydrophobic cleft in the N-terminal lobe of cTnC.

More recently, an electron cryomicroscopy structure of the cardiac muscle thin filament in the Ca^{2+}-bound state has been determined at 4.8 Å resolution (Yamada *et al.*, 2020). The structure shows a similar cTnC–cTnI interaction, with the cTnI switch α-helix running in the same antiparallel direction across the cleft.

Because of the weak association of the troponin C and I subunits (K_d of ∼200 μ*M*; Pineda-Sanabria *et al.*, 2013), structural models of the native troponin complex have been difficult to achieve. As a tool to obtain high-resolution NMR structures of the complex, cardiac cTnC–cTnI chimeric proteins have been designed in which the N-terminal domain of troponin C is fused to the C-terminal 'switch' region of troponin I (Pineda-Sanabria *et al.*, 2014). The use of a chimera greatly increases the effective concentration and promotes the stabilization of the cTnI switch region. Using such a chimeric protein, a number of NMR structures have been determined (Pineda-Sanabria *et al.*, 2014; Cai *et al.*, 2016, 2018). These structures show an interaction between cTnC and cTnI similar to that seen in the native structure, with the cTnI portion forming an approximately three-turn helix running antiparallel to the cTnC portion of the chimera. The cTnI peptide does not completely cover the hydrophobic groove of the cTnC domain, leaving a small portion of it exposed.

To better understand the interactions of the cTnI peptide with the cTnC domain, we undertook X-ray crystallographic studies of cTnC–cTnI chimera proteins. Using two variants of the cTnC–cTnI chimera protein, we obtained high-resolution crystal structures of the chimera proteins in two different crystal forms. In this paper, we present the three-dimensional crystal structures of these two chimera variants and report the observation of novel interactions between the cTnC domain and the cTnI helix.

2. Materials and methods

2.1. Preparation of untagged cTnC–cTnI chimera: cTnC(1–90)-C35S-C84S–cTnI(136–163)

A clone was prepared that included the N-terminal domain of human cardiac troponin C (residues 1–90 with C35S and C84S mutations) linked to the C-terminal region of troponin I (residues 136–163), based on the NMR chimera construct (Cai *et al.*, 2016), in pET-28 vector (Table 1). The clone was expressed in *Escherichia coli* BL21 (DE3) cells (Novagen) at 37°C in LB medium to an OD_{600} of 1.0 and was then induced using 1 m*M* isopropyl β-D-1-thiogalactopyranoside (IPTG) at 37°C for 3 h.

All steps were performed at 4°C using an ÄKTA pure M1. Frozen cells harvested from 2 l of culture were suspended in 50 ml lysis buffer [20 m*M* Tris pH 7.5, 300 m*M* NaCl, 10 m*M* $MgSO_4$, 1 m*M* $CaCl_2$, 1 m*M* DTT, one tablet of cOmplete EDTA-free protease-inhibitor cocktail (Roche Applied Science) and 20 units per millilitre of benzonase nuclease (EMD Millipore)]. The cells were lysed by sonication. The lysate was clarified by sedimentation at 30 000*g* for 30 min (Thermo F21-8x50y rotor) and the supernatant was diluted

Table 1
Sequences of the constructs used.

Untagged cTnC–cTnI chimera protein: cTnC(1–90)-C35S-C84S–cTnI(136–163)	
Length	118 amino acids
Molecular weight (Da)	13283
Complete amino-acid sequence of the construct produced	MDDIYKAAVEQLTEEQKNEFKAAFDIFVLGAED GSISTKELGKVMRMLGQNPTPEELQEMIDEVD EDGSGTVDFDEFLVMMVRSMKDDSKGKFKRPT LRRVRISADAMMQALLGARAK
C-terminally His-tagged cTnC–cTnI chimera protein: cTnC(1–90)-C35S-C84S–cTnI(136–163)-His	
Length	125 amino acids
Molecular weight (Da)	14162
Complete amino-acid sequence of the construct produced	MDDIYKAAVEQLTEEQKNEFKAAFDIFVLGAED GSISTKELGKVMRMLGQNPTPEELQEMIDEVD EDGSGTVDFDEFLVMMVRSMKDDSKGKFKRPT LRRVRISADAMMQALLGARAKGHHHHHH

sixfold in buffer *A* (20 m*M* Tris pH 7.5, 1 m*M* DTT, 1 m*M* $CaCl_2$) and loaded onto a 5 ml HiTrap Q FF (GE Healthcare) column equilibrated with buffer *A*. The column was washed with ten volumes of buffer *A* and the protein was eluted with a linear gradient of 0–700 m*M* NaCl in buffer *A*. Fractions were pooled and loaded onto a HiLoad 26/60 Superdex 200 column (GE Healthcare) equilibrated with buffer *B* (20 m*M* Tris pH 7.5, 300 m*M* NaCl, 0.1 m*M* $CaCl_2$, 1 m*M* DTT). The protein eluted as a monomer. The final yield of purified cTnC(1–90)-C35S-C84S–cTnI(136–163) protein was 80 mg per litre of culture. The protein purity was ≥98% as determined by SDS–PAGE analysis and Coomassie Brilliant Blue staining (data not shown). Electrospray ionization mass spectrometry confirmed the identity of the protein. Purified cTnC(1–90)-C35S-C84S–cTnI(136–163) was spiked with 1 *M* $CaCl_2$ to give a final concentration of 10 m*M* $CaCl_2$ and concentrated to 41.6 mg ml^{-1} in 20 m*M* Tris pH 7.5, 300 m*M* NaCl, 10 m*M* $CaCl_2$, 1 m*M* DTT. Crystals were grown at 20°C in sitting drops from 1 μl protein solution mixed with 1 μl well solution consisting of 0.1 *M* sodium acetate pH 4.5, 0.2 *M* ammonium acetate, 16–20% PEG 4K. The crystals appeared spontaneously within 1–2 weeks. Seeding with previously obtained crystals improved the reproducibility and the speed of crystal formation. The crystals were flash-cooled in liquid nitrogen in cryosolution consisting of 75% well solution and 25% ethylene glycol.

2.2. Preparation of C-terminally histidine-tagged cTnC–cTnI chimera: cTnC(1–90)-C35S-C84S–cTnI(136–163)-His

A second clone was prepared that included a C-terminal histidine tag (Table 1) in order to precisely mimic the protein used in the reported NMR structure (Cai *et al.*, 2018), expressed and lysed as described above. Instead of loading onto a Q column, the protein was loaded onto a 5 ml HisTrap FF (GE Healthcare) column equilibrated with buffer *A* (20 m*M* Tris pH 8, 300 m*M* NaCl, 1 m*M* $CaCl_2$, 1 m*M* DTT, 20 m*M* imidazole). The column was washed with ten volumes of buffer *A* and the protein was eluted with a linear gradient of 20–400 m*M* imidazole in buffer *A*. Fractions were pooled and loaded onto a HiLoad 26/60 Superdex 200 column (GE Healthcare) equilibrated with buffer *B* (20 m*M* Tris pH 8,

Table 2
Data collection and processing.

Values in parentheses are for the highest resolution shell.

	Tetragonal (form 1), untagged chimera, PDB entry 7sc2	Orthorhombic (form 2), His-tagged chimera, PDB entry 7sc3
Diffraction source	Beamline 17-ID, APS	Beamline 17-ID, APS
Wavelength (Å)	1.000	1.000
Temperature (K)	100	100
Detector	Dectris PILATUS 6M	Dectris PILATUS 6M
Crystal-to-detector distance (mm)	300	450
Rotation range per image (°)	0.25	0.25
Exposure time per image (s)	0.078	0.078
Data-reduction program	*autoPROC* 1.1.7	*autoPROC* 1.1.7
Crystallographic space group	$P4_32_12$	$P2_12_12_1$
a, b, c (Å)	40.94, 40.94, 128.93	38.85, 40.96, 67.00
α, β, γ (°)	90, 90, 90	90, 90, 90
Ansiotropic resolution range (Å)	39.02–1.81 (1.95–1.81)	34.95–2.26 (2.51–2.26)
Total No. of reflections	102388 (5198)	20501 (1270)
No. of unique reflections	8344 (417)	3437 (202)
Completeness (ellipsoidal) (%)	93.4 (50.9)	88.5 (55.2)
Multiplicity	12.3 (12.5)	6.0 (6.3)
$\langle I/\sigma(I)\rangle$	12.9 (0.3)	5.5 (1.1)
$R_{\rm r.i.m.}$	0.073 (2.447)	0.276 (1.859)
Overall B factor from Wilson plot (Å^2)	48.41	41.97

Table 3
Structure refinement.

Values in parentheses are for the highest resolution shell.

	Tetragonal (form 1), untagged chimera, PDB entry 7sc2	Orthorhombic (form 2), His-tagged chimera, PDB entry 7sc3
Refinement program	*BUSTER-TNT* 2.11.7	*BUSTER-TNT* 2.11.7
Resolution range (ansiotropic) (Å)	39.02–1.814 (1.94–1.81)	34.95–2.229 (2.65–2.23)
Completeness (anisotropic) (%)	93.5	88.5
No. of reflections, working set	8344 (384)	3437 (409)
No. of reflections, test set	422 (14)	165 (22)
Final $R_{\rm cryst}$	0.222 (0.234)	0.243 (0.198)
Final $R_{\rm free}$	0.239 (0.207)	0.278 (0.226)
No. of non-H atoms		
Protein	803	776
Ion	1	1
Solvent	28	8
Total	833	788
R.m.s. deviations		
Bonds (Å)	0.008	0.009
Angles (°)	0.83	0.97
Average B factor (Å^2)		
Protein	50.3	38.5
Ion	49.9	48.1
Water	57.3	33.3
Ramachandran plot		
Favored regions (%)	98.2	96.3
Additionally allowed (%)	0.9	2.8

300 m*M* NaCl, 1 m*M* $CaCl_2$, 1 m*M* DTT). The protein eluted as a monomer. The final yield of purified cTnC(1–90)-C35S-C84S–cTnI(136–163)-His protein was 48 mg per litre of culture. The protein purity was ≥98% as determined by SDS–PAGE analysis and Coomassie Brilliant Blue staining (data not shown). Electrospray ionization mass spectrometry confirmed the protein identity.

The purified cTnC(1–90)-C35S-C84S–cTnI(136–163)-His was spiked with 1 *M* $CaCl_2$ to give a final concentration of 10 m*M* $CaCl_2$ and concentrated to 33 mg ml^{-1}. Crystallization drops were set up with the conditions used for the nontagged chimera at room temperature. Crystals appeared overnight after cross-seeding from the nontagged chimera crystals.

2.3. Data collection, processing and structure determination

Data were collected on a PILATUS 6M detector at a temperature of 100 K on beamline 17-ID at the Advanced Photon Source (APS), Argonne National Laboratory. The data were processed and scaled using *autoPROC* (Vonrhein *et al.*, 2011). The data-collection parameters are given in Table 2. Molecular-replacement searches were performed with *MOLREP* (Vagin & Teplyakov, 2010), *Phaser* (McCoy *et al.*, 2007) and *BALBES* (Long *et al.*, 2008) from the *CCP*4 suite of programs. The structure was refined using routine *autoBUSTER* (Global Phasing Ltd, Cambridge, UK) alternating with manual building with *Coot* (Emsley *et al.*, 2010). The refinement parameters are given in Table 3. The cTnC–cTnI chimera structures in both crystal forms have been deposited in the Protein Data Bank (PDB entries 7sc2 and 7sc3).

3. Results

3.1. Structure determination of the untagged chimera protein: cTnC(1–90)-C35S-C84S–cTnI(136–163)

The untagged protein crystallized in the tetragonal Laue group 4/*mmm*. The reduced anisotropic structure-factor data file was 93.4% complete to 1.81 Å resolution (Table 2). Molecular-replacement models were prepared based on the reported NMR structures of the cTnC–cTnI chimera, including Protein Data Bank (PDB) entries 5vln (Cai *et al.*, 2016) and 6mv3 (Cai *et al.*, 2018). Additional models were made based on the NMR structures of the cTnC–cTnI complex (PDB entry 2mkp; Robertson *et al.*, 2014) as well as the corresponding region of the crystal structure of the troponin core domain (PDB entry 1j1e; Takeda *et al.*, 2003).

Molecular-replacement searches performed with *MOLREP* and *Phaser* failed to give a solution using any of the atomic models. However, using only the N-terminal domain of troponin C alone, without the troponin I peptide, as a search model gave a clear solution for that portion of the chimera. The electron-density difference maps showed a well defined, approximately six-turn, α-helix running across the hydrophobic face of the cTnC domain. This helix was longer and did not correspond to the position of the cTnI helix in any of the NMR or X-ray models used in the molecular-replacement searches. Further attempts using a two-step procedure, first determining and fixing the cTnC domain position and then attempting to determine the orientation of the cTnI peptide using the cTnI portion of the chimera structure, also failed to provide an acceptable solution.

The automated molecular-replacement routine *BALBES* was then used in an attempt to determine the structure. The program first selected the structure of the N-terminus of the Ca^{2+}-bound, open form of cTnC (PDB entry 1wrk; S. Takeda, T. Igarashi, Y, Oishi & H. Mori, unpublished work) to determine the location of the cTnC domain. The resulting position was similar to the partial molecular-replacement solution determined previously. The program then selected an extended α-helix from a synthetic α-helical bundle (PDB entry 3hez; W. S. Horne & S. H. Gellman, unpublished work) as the search molecule for the cTnI peptide, even though it had only 28% sequence similarity to the cTnI peptide. The combined model containing the entire cTnC domain and an 18-residue α-helix of the cTnI peptide, but not the linker region, gave a solution with an initial *R* factor of 28.0% (R_{free} = 48.1%) with a *BALBES Q*-factor of 0.684. After refinement, the structure had an *R* factor of 22.2% (R_{free} = 23.9%) for 803 protein atoms and 28 solvent molecules.

The cTnC domain portion of the chimera structure is in the open 'Ca^{2+}-saturated' conformation that closely matches the NMR chimera structure. However, there were significant differences in the cTnI peptide region. The peptide is in an extended six-turn α-helical conformation approximately twice as long as that observed in the previous published structures, completely covering the hydrophobic groove of the cTnC domain, and running in the opposite direction to the helix seen in the other structures. Attempts to refit the helix in the expected antiparallel orientation were unsuccessful.

There was no clear electron density for the linker region between the cTnC domain and the cTnI peptide. This is not surprising since the linker is the most flexible region in the NMR structure. However, the missing residues of the linker are not long enough to connect the C-terminal end of the cTnC domain to the N-terminal end of the cTnI helix within the same molecule, a distance of ∼20 Å.

3.2. Structure determination of the C-terminally histidine-tagged protein: cTnC(1–90)-C35S-C84S–cTnI(136–163)-His

The protein used in the structure determination of the untagged cTnC–cTnI chimera differs from the construct reported for the NMR structure in the removal of the C-terminal His tag. Since our crystal structure of the untagged cTnC–cTnI chimera showed a different cTnI orientation relative to the reported structures, there was a possibility that this difference might be due to the six-residue tag. To test this possibility, the protein was prepared and crystallized and the structure was determined using C-terminally His-tagged protein with an identical sequence to that used in the NMR structure. Although the tagged protein was crystallized by cross-seeding from the nontagged chimera, and grew under similar conditions, the crystals had a different morphology (Fig. 1) and, unlike the plate-like tetragonal crystals, grew as needles. These crystals have the symmetry of the orthorhombic Laue group *mmm* and the anisotropic structure-factor data file was 88.5% complete to 2.26 Å resolution (Table 2).

The structure was determined with routine *MOLREP* using the untagged cTnC–cTnI chimera structure as the model in the molecular-replacement search. The routine gave a single solution (CC = 0.6006) in space group $P2_12_12_1$. The structure was refined in a similar fashion as the untagged protein. The final structure has an *R* factor of 24.3% (R_{free} = 27.8%) for 776 protein atoms and eight solvent molecules (Table 3).

The orthorhombic crystal form of the chimera shares similar features with the tetragonal form, such as the open 'Ca^{2+}-saturated' conformation of the cTnC domain and the cTnI helix running in a parallel orientation. However, in this crystal form there is better defined difference electron density for the linker region, allowing complete tracing of the protein chain. Unexpectedly, the electron density indicates that the linker region is pointing away from the cTnC domain, and the cTnI peptide does not interact with the cTnC domain that it is linked to but rather with the hydrophobic groove of an adjacent cTnC domain in the crystal structure (Fig. 2). This observation explains how the short linker is able to connect the cTnC domain to the cTnI helix. Instead of reaching across a distance of ∼20 Å, it only needs to connect a distance of ∼7 Å. The final four C-terminal residues of the cTnC peptide, along with the six-residue His tag, are not seen in the structure.

Examination of the packing of the molecules in the initial tetragonal crystal form shows a symmetry-related cTnI peptide close to the cTnC domain, requiring the missing linker

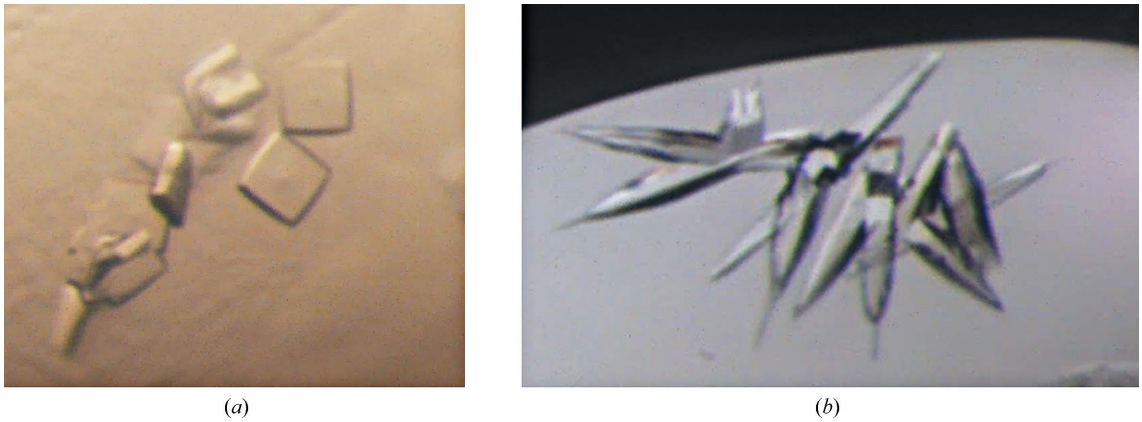

(*a*) (*b*)

Figure 1
The crystals used in the present study. Photographs of (*a*) the tetragonal and (*b*) the orthorhombic crystals used in the present study.

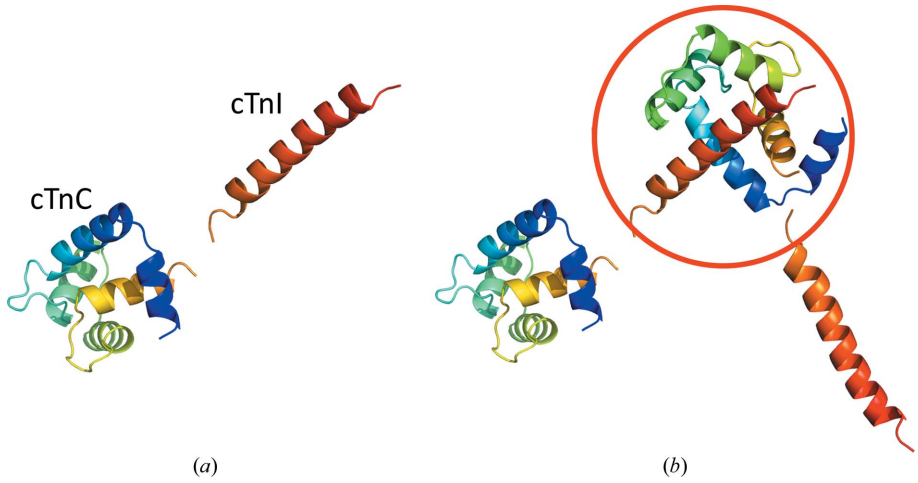

Figure 2
Position of the cTnI peptide in an adjacent molecule. (*a*) Ribbon drawing of the chimera structure showing the extended orientation of the cTnI peptide. (*b*) Overlay of the structure with the symmetry-related molecule showing the domain swapping, with the unique region circled.

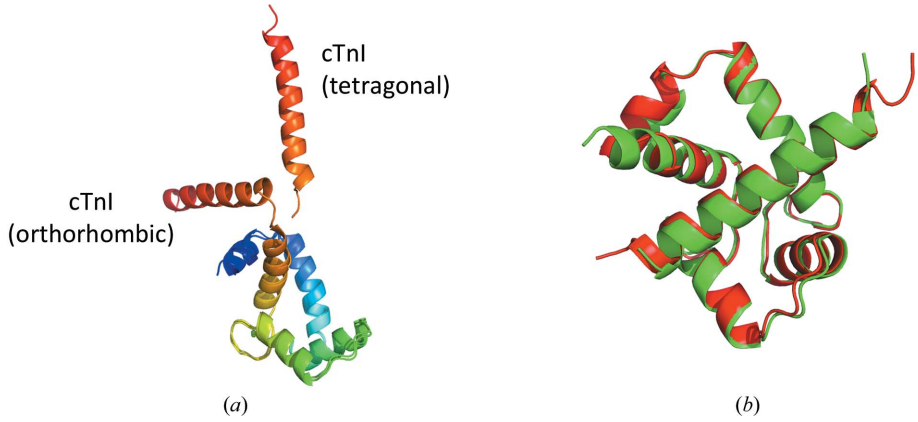

Figure 3
Comparison of the linker orientations in the two crystal forms. (*a*) Overlay of the cTnC domains in the two crystal forms showing the different orientations of the cTnI peptides. (*b*) Overlay of the two structures showing the position of the cTnI peptide in the symmetry-related molecule (red, orthorhombic form; cyan, tetragonal form).

to span only a distance of ∼7 Å. While there is no contiguous electron density to confirm this hypothesis, it suggests that as in the orthorhombic form the cTnI peptide in this structure has flipped around and is interacting with the cTnC domain of an adjacent molecule. Due to the differences in the packing of the molecules in the two crystal forms, the linkers are in different conformations in order for the cTnI peptide to interact with the cTnC domains of the adjacent molecules (Fig. 3).

In both crystal forms, the cTnI peptide is in an extended α-helix conformation and runs in a 'parallel' orientation across the entire hydrophobic face of the cTnC domain. The residues involved in the cTnC–cTnI interaction in the two structures are similar. In both cases, however, there is a single hydrogen-bond interaction between the carboxyl group of Leu48 in the TnC domain and the side-chain N atom of Arg147 in the cTnI region.

4. Discussion

The X-ray crystal structure of a human cardiac muscle troponin C–troponin I (cTnC–cTnI) chimera has been determined in two different crystal forms at better than 2.2 Å resolution. The N-terminal domain of cTnC is in the open 'Ca^{2+}-saturated' conformation with a hydrophobic groove running across one face. In this regard, the cTnC domains in the X-ray and NMR chimera structures are essentially identical (r.m.s.d. of ∼1.35 Å). The main differences between these structures are the conformation, length and orientation of the cTnI peptide that lies across the face of the cTnC hydrophobic groove.

4.1. Domain swapping

In the crystal structures, the cTnI peptide interacts with the hydrophobic groove of a cTnC domain in an adjacent molecule in the crystal structure (Fig. 3). There are numerous examples of 'domain swapping' in crystal structures (Liu & Eisenberg, 2002). In this case, the domain swapping may be due to the fact that the linker between the domains is not long enough for the cTnI peptide to make the preferred interactions with the cTnC domain within the same molecule. However, in the crystal structure, the peptide can swing around and bind to the cTnC domain of an adjacent molecule.

The chimera molecules do not form dimers by swapping domains with each other. Rather, the helical domain of one molecule interacts with the globular domain of an adjacent molecule, effectively building up a structure of interconnected molecules.

4.2. Directionality of the troponin I peptide

A number of previous studies indicate that the two lobes of troponin C interact with opposite ends of the inhibitory region of troponin I, suggesting an 'antiparallel' orientation of the cTnI peptide with respect to cTnC (Farah & Reinach, 1995). In both of the crystal structures in our study the cTnI peptide lies across the face of the cTnC hydrophobic groove in a 'parallel' orientation.

There are several unique features of the cTnI fragment that confirm the unexpected orientation of the α-helix observed in the crystal structures. Phe138 is the only aromatic residue and Pro141 is the only proline in the cTnI peptide. Electron density for both residues is clearly seen in the structure (Fig. 4). Except for the ends of two arginine side chains and the two C-terminal residues, all of the side chains in the helix are evident in the electron-density map.

It should be noted that much of the evidence for the orientation of the troponin C and troponin I subunits is based on studies of skeletal muscle. These studies suggest that the TnI peptide lies across the face of the TnC hydrophobic groove in an antiparallel fashion (Farah & Reinach, 1995), and all of the previous structural work with the cardiac TnI peptide is consistent with this model. However, one must be very careful in extrapolating results from skeletal muscle to cardiac muscle troponin without firm evidence, as the mode of interaction in the two systems may be very different. In the NMR structure of the complex of the cTnC N-terminal domain and the cTnI C-terminal 'switch' peptide (Li *et al.*, 1999) the authors note a lack of restraints for the cTnI peptide and that the backbone atoms have a high r.m.s.d.. In the crystal structure of the human cardiac troponin core domain (Takeda *et al.*, 2003) the electron density associated with the switch region was 'not well defined', and in the cryoEM structure of the cardiac muscle thin filament (Yamada *et al.*, 2020) the density for cTnI in this region 'mostly disappears' in the Ca^{2+}-bound state. Given the flexibility of both the cTnC inter-domain region and the cTnI switch peptide, a parallel orientation of the cTnI peptide across the hydrophobic face of the N-terminal domain of cTnC is clearly possible.

4.3. Length of the cTnI helix

In the NMR structures, the cTnI peptide forms a ten-residue, three-turn α-helix (residues 150–159) sandwiched between two random-coil sections. The chimera crystal structures contain a much longer, 26-residue α-helix (residues 134–163) (Fig. 5). In the solution structure of the N-terminal domain of human cardiac cTnC with the cTnI C-terminal 'switch' peptide (Li *et al.*, 1999), the end of the cTnC domain is approximately 12 Å from the start of the cTnI peptide. The cTnC–cTnI chimera (Pineda-Sanabria *et al.*, 2014) contains six residues between the cTnC domain and the cTnI peptide, which would be long enough to link to the two domains, provided that the cTnI peptide is running in the antiparallel direction. However, if the cTnI peptide is running in the opposite direction, the ends of the domains would be too far apart to be properly linked. Thus, in solution the peptide may be forced into an antiparallel orientation which permits only a shorter helix to form.

4.4. Interactions between the cTnC domain and the cTnI peptide

In the chimera crystal structures, the single six-turn α-helix runs completely across the hydrophobic groove, and the interaction has an excluded surface area of ~700 $Å^2$. There is a single hydrogen-bond interaction between the cTnC domain (Leu48) and the cTnI peptide (Arg147). This interaction is seen in both crystal forms and could be the 'switch' that is formed upon calcium binding, holding the cTnC in the active conformation. The remaining interactions mostly consist of long-range hydrophobic interactions (>3.2 Å) across the entire face of the cTnC groove (Fig. 6). The lack of a strong interaction between the two is not surprising given the high dissociation constant ($K_d \simeq 200\ \mu M$). In addition to the hydrophobic interactions with the cTnC domain, the cTnI

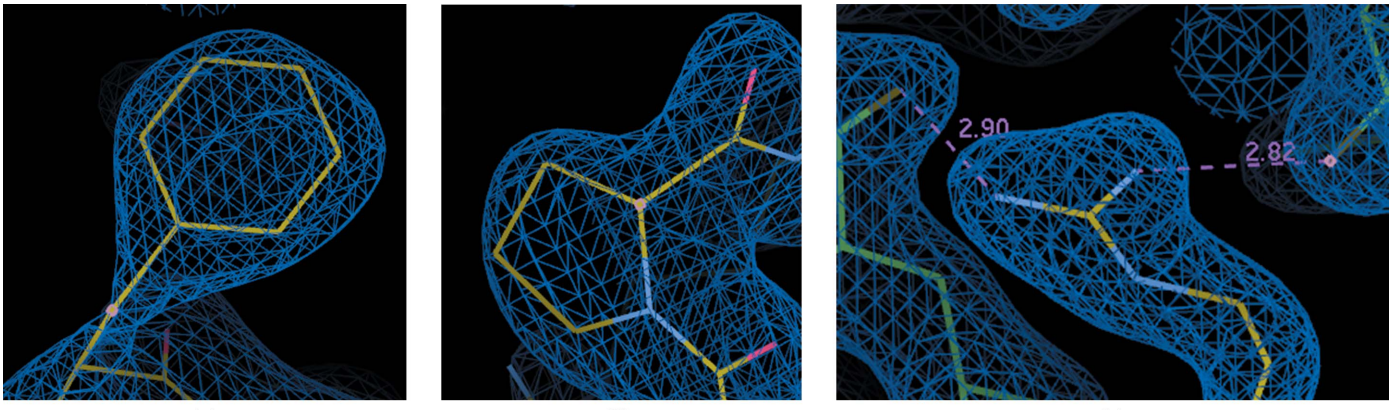

(*a*) (*b*) (*c*)

Figure 4
Electron-density drawings. $2F_o - F_c$ electron-density maps of residues (*a*) Phe138, (*b*) Pro141 and (*c*) Arg147 in the chimera structure.

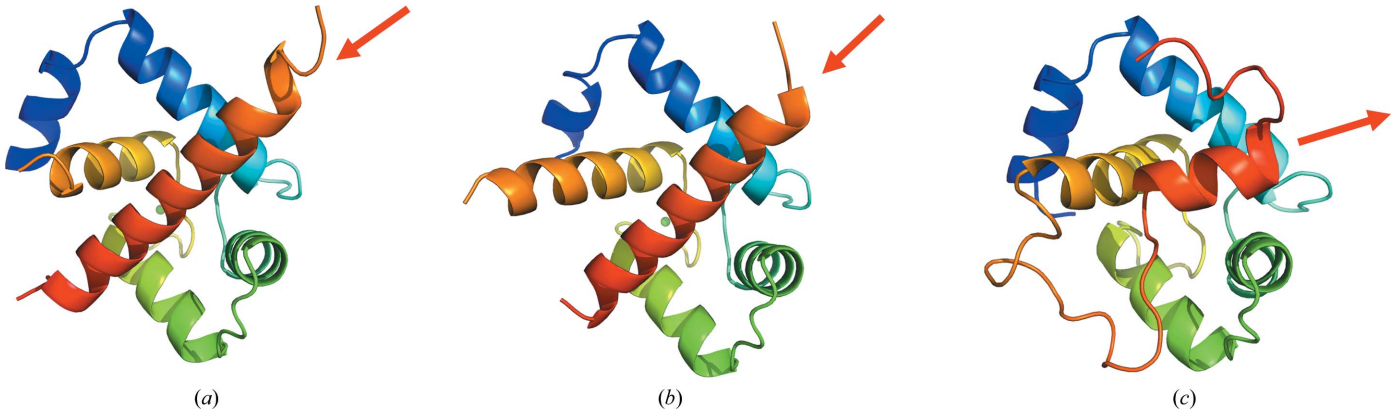

Figure 5
Structure of the troponin chimera (ribbon drawing). Comparison of the chimera structures. Ribbon drawings are shown for (*a*) the X-ray structure of the tetragonal form, (*b*) the X-ray structure of the orthorhombic form and (*c*) the NMR structure. The arrows indicate the direction of the cTnI peptide.

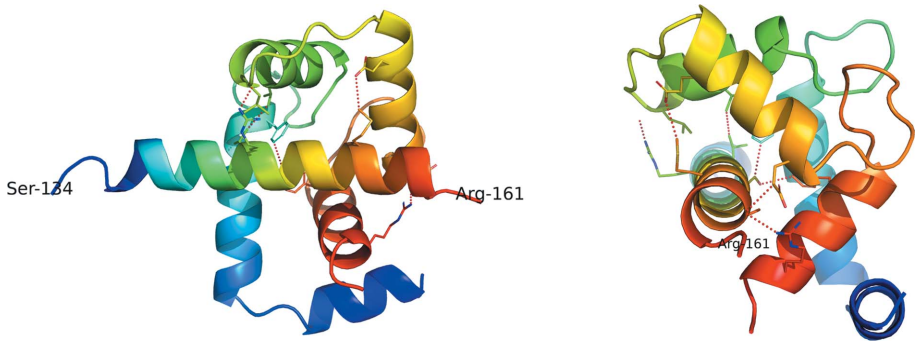

Figure 6
Details of the cTnC–cTnI Interface. Perpendicular views show the interactions between the cTnI helix and the cTnC domain in the chimera crystal structure (tetragonal form).

peptide makes a number of interactions with residues in symmetry-related molecules, including numerous hydrogen bonds. These are seen in both crystal forms of the chimera and presumably help to stabilize the helix in the observed orientation. The same orientation is observed in two different crystal forms, suggesting that this not solely an artifact of protein crystallization. Given the weak interaction between the cTnC domain and the cTnI peptide, there may be multiple conformations of the cTnC–cTnI hydrophobic groove interaction which may be important to perform the rapid switching required by cardiac muscle.

4.5. Ligand binding to the chimera

In NMR structures of the cTnC–cTnI chimera bound to ligands such as bepridil (Wang *et al.*, 2002) and W7 (Cai *et al.*, 2018), the binding site on the hydrophobic groove of cTnC includes Leu41, Leu48, Met60 and Met80. In the NMR structures, these residues of the hydrophobic core are exposed and movement of the cTnI peptide is not required for the ligand to bind. In the crystal structure, in which the cTnI α-helix extends across the entire face of the cTnC hydrophobic groove, the ligand-binding site is precluded by the positions of residues 149–153 in the cTnI helix. Thus, the cTnI peptide would have to be displaced in some way in order for ligand binding.

5. Conclusions

The structural details of the intramolecular interactions in cardiac troponin have been difficult to obtain due to the weak binding between the subunits. While a number of different experimental techniques have been used to provide important details, each has limitations that have prevented a clear, cohesive model of this system. Moreover, much of the data used to define the model has come from other tissues or species which may have different mechanisms to that found in human cardiac muscle.

The structures presented here are from a chimera protein in which the N-terminal domain of cTnC (residues 1–90) is fused to the switch region of cTnI (residues 134–163). Keeping these two segments in close proximity allowed biochemical and structural studies that were difficult to perform using separate proteins. However, the chimera is an artificial hybrid protein and may not represent the interaction *in situ*. As such, one must be cautious when analyzing results obtained from such a system.

We do not suggest that there is any type of domain swapping or dimerization of the troponin molecules in intact muscle fibers. Rather, the chimera protein was designed as an efficient way to obtain high-resolution NMR structures of the interaction between the troponin subunits and has been used to determine the binding mode of a number of drugs to this

interface. We believe that the crystal structure of this protein may also be helpful in understanding these interactions.

Hopefully, the current study has provided information to help clarify the structural aspects of the troponin system. Differences between the crystal and NMR structures suggest that there may be multiple states of the conformation between the proteins in the cardiac troponin complex. Clearly, further studies are needed to elucidate the details of this interaction.

Acknowledgements

The authors would like to thank Mian Gao for providing the clones and Zachary Cohen for expression of the proteins used in this work. We would also like to thank Jodi Muckelbauer, Brett Beno, Sean Little, Michael Myers, Danielle Aubele and members of the Troponin Activator group at Bristol Myers Squibb for useful discussions. We thank the staff of the IMCA-CAT for assistance in data collection. Use of the IMCA-CAT beamline 17-ID at the Advanced Photon Source was supported by the companies of the Industrial Macromolecular Crystallography Association through a contract with Hauptman–Woodward Medical Research Institute. This research used resources of the Advanced Photon Source, a US Department of Energy (DOE) Office of Science User Facility operated for the DOE Office of Science by Argonne National Laboratory under Contract No. DE-AC02-06CH11357.

References

Cai, F., Hwang, P. M. & Sykes, B. D. (2018). *Biochemistry*, **57**, 6461–6469.

Cai, F., Li, M. X., Pineda-Sanabria, S. E., Gelozia, S., Lindert, S., West, F., Sykes, B. D. & Hwang, P. M. (2016). *J. Mol. Cell. Cardiol.* **101**, 134–144.

Emsley, P., Lohkamp, B., Scott, W. G. & Cowtan, K. (2010). *Acta Cryst.* D**66**, 486–501.

Farah, C. S. & Reinach, F. C. (1995). *FASEB J.* **9**, 755–767.

Li, M. X., Spyracopoulos, L. & Sykes, B. D. (1999). *Biochemistry*, **38**, 8289–8298.

Liu, Y. & Eisenberg, D. (2002). *Protein Sci.* **11**, 1285–1299.

Long, F., Vagin, A. A., Young, P. & Murshudov, G. N. (2008). *Acta Cryst.* D**64**, 125–132.

Marston, S. & Zamora, J. E. (2020). *J. Muscle Res. Cell Motil.* **41**, 71–89.

McCoy, A. J., Grosse-Kunstleve, R. W., Adams, P. D., Winn, M. D., Storoni, L. C. & Read, R. J. (2007). *J. Appl. Cryst.* **40**, 658–674.

Pineda-Sanabria, S. E., Julien, O. & Sykes, B. D. (2014). *ACS Chem. Biol.* **9**, 2121–2130.

Pineda-Sanabria, S. E., Robertson, I. M., Li, M. X. & Sykes, B. D. (2013). *Cardiovasc. Res.* **97**, 481–489.

Robertson, I. M., Pineda-Sanabria, S. E., Holmes, P. C. & Sykes, B. D. (2014). *Arch. Biochem. Biophys.* **552–553**, 40–49.

Takeda, S., Yamashita, A., Maeda, K. & Maéda, Y. (2003). *Nature*, **424**, 35–41.

Vagin, A. & Teplyakov, A. (2010). *Acta Cryst.* D**66**, 22–25.

Vonrhein, C., Flensburg, C., Keller, P., Sharff, A., Smart, O., Paciorek, W., Womack, T. & Bricogne, G. (2011). *Acta Cryst.* D**67**, 293–302.

Wang, D., Li, M. X. & Sykes, B. D. (2002). *J. Biol. Chem.* **277**, 31124–31133.

Yamada, Y., Namba, K. & Fujii, T. (2020). *Nat. Commun.* **11**, 153.